EFFICIENT DRIVES FOR SINGLE-PHASE AC MOTORS: ANALYSIS AND APPLICATIONS

Juan F. Gallego-Calderon, California State University Fresno; Nagy Bengiamin, California State University Fresno

Abstract

In this paper, the authors present an energy efficiency study of Variable-Speed Drives for Single-Phase Induction Motors. The objective was to evaluate popular variable-speed drive schemes as they operate in their most efficient mode under different loading conditions. The considered schemes included phase control, variable-frequency drives and voltage control. This study focused on the development of experimental test methodologies to characterize motors and implement desired control schemes. Mathematical modeling and computer simulations were also utilized for engineering design and analysis. The fan load application was considered for further illustration of the developed methodology. This study provides a general framework for the evaluation and selection of variable-speed drives.

Introduction

Speed control of AC motors evolved very rapidly with advances in power electronics technology [1]. Applications that were dominated by DC motors became most suited for AC motors as a more economical alternative. Three-phase motors, however, were the prime candidates for initial developments for their more significant impact on high-power industrial applications. With the maturing of three-phase motor drives, technologies started to find their way to single -phase motor applications which constitute the largest percentage of electric power consumption in commercial and residential applications. AC Single-Phase Induction Motors (SPIMs) are popular for their low cost and versatility. Compared to three-phase induction motors, single-phase motors lack the self-starting capabilities and they are more sensitive to loading conditions.

For applications with varying loads, a variable-speed drive is a must since it can achieve up to 50% in energy savings. This principle often applies to machines that need to be constantly starting. By means of variable-speed drives, it is possible to regulate the starting current of such machines and, therefore, save more energy [2]. There are three commonly known techniques for AC motor drives; namely, variable frequency [3], voltage control [4], [5] and variable rotor resistance. Several studies have been conducted to analyze the performance of the different drives.

Nomenclature

R_1, X_1	Resistance and reactance of the stator
R'_2, X'_2	Resistance and reactance of the rotor
X_m	Mutual reactance
τ_{ind}	Induced torque
V_{TH}, R_{TH}	Thévenin voltage and resistance
ω_m, ω_{sync}	Motor speed and synchronous speed in rad/sec
I	Stator current
Z_F, Z_B	Forward and backward impedance
P_{in}, P_{out}	Input and output power
P_{AG}, $P_{AG,F}$, $P_{AG,B}$	Air-gap power: total, forward and backward
P_{conv}	Converted power
P_{RCL}	Core losses
P_{rot}	Rotational losses
P_s	Power savings
f	Line frequency in Hz ($\omega=2\pi f$)
V	Phase voltage
τ	Torque
n_m, n_{sync}	Motor speed and synchronous speed in rpm
s	Slip
$p.f.$	Power factor
η	Efficiency

In this paper, the theory behind the steady-state operation of SPIM is presented and was used for the mathematical models development in this study. Experimental tests were then performed in order to determine the motor parameters. The torque-speed motor characteristic was used to validate experimental results of the motor-winding parameters. Power consumption under different loading conditions was ana-

lyzed experimentally and via modeling techniques for different control schemes under varying loading conditions to find the optimal mode of operation. Moreover, the fan application was analyzed in order to provide a real-life application where this kind of analysis is important for energy efficiency.

Induction-Motor Model

In applications where there is insufficient information available about the motor parameters, such as winding resistance and inductance, it is necessary to execute the following three classical tests: DC test, locked-rotor test and the no-load test. These experimental tests are based on the single-phase induction-motor static RC equivalent circuit model presented in Figure 1. This model is based on the double-revolving-field theory. This theory states that a stationary pulsating magnetic field can be expressed as two rotating magnetic fields (forward and backward) of the same magnitude but with different direction. The effective torque that is produced is then practically equal to the resultant sum of the torque components due to each of the two magnetic fields [6].

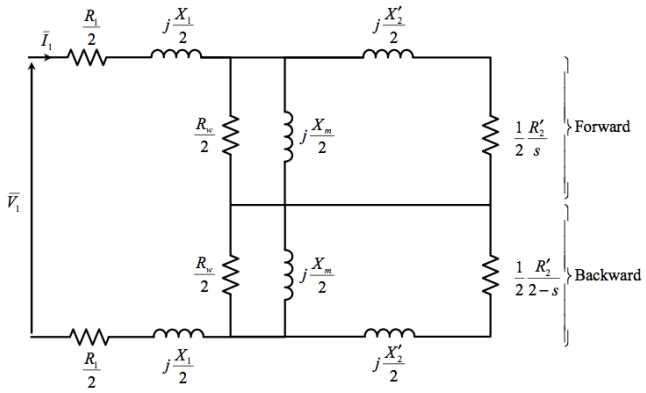

Figure 1. Equivalent Circuit of a Single-Phase Induction Motor

Since the purpose of this study was to analyze the energy efficiency of the drives discussed earlier, it was not necessary to analyze the dynamics of the induction motor. This is where the d-q model would have been necessary. The motor -winding parameters found experimentally are shown in Table 1.

This section describes the relationship of the motor's torque, power and speed. Chapman [6] derived the formula that describes the induced torque from an analysis of the three-phase motor's equivalent circuit. This formula can be applied to the single-phase motor using a 1/3 scaling factor since the torque is additive. Thus, this formula was applied here using the parameters presented in Table 1. In addition, the ideal torque-speed characteristic was compared with experimental data for validity.

Table 1. Induction-Motor Parameters

Parameter	Value
Main winding stator resistance (ohms)	15.8971
Main winding stator/rotor reactance (ohms)	17.9800
Main winding stator/rotor inductance (H)	0.0477
Main winding rotor resistance (ohms)	12.7190
Main winding mutual reactance (ohms)	223.1849
Main winding mutual inductance (H)	0.5920

It should be noted from Equation (1) that the produced torque is dependent on the slip (motor speed), operating frequency as it affects the reactance ($X=j\omega L$), and the phase voltage, V_ϕ. The resistance also plays a role, but it was assumed constant for purposes of this study. Most economical SPIMs are of the squirrel-cage type, where the rotor resistance is practically fixed. Wound-rotor motors may provide access terminals to change their effective rotor resistance. The dependence of τ_{ind} on n_m, V_ϕ, f and R_2 permits the reverse logic of adjusting n_m for a given τ_{ind} (load) using V_ϕ and f.

$$\tau_{ind} = \frac{\frac{V_{TH}^2 R_2}{s}}{\omega_{sync}\left[\left(R_{TH}+\frac{R_2}{s}\right)^2+(X_{TH}+X_2)^2\right]} \quad (1)$$

where

$$V_{TH} \approx V_\varphi \frac{X_M}{X_1+X_M}$$

$$R_{TH} \approx R_1\left(\frac{X_M}{X_1+X_M}\right)^2$$

Equation (1) was utilized to create the torque-speed characteristic curve presented in Figure 2, where $s = (n_m-n_{sync})/n_{sync}$. In physical experiments, the motor was operated under a variable load and the torque was measured at the corresponding speeds (see Figure 2). The rated motor voltage (115 V) and nominal frequency (60 Hz) were used in this test. Figures 3 and 4 show the simulation results for the same motor for variable f and $V\phi$, respectively.

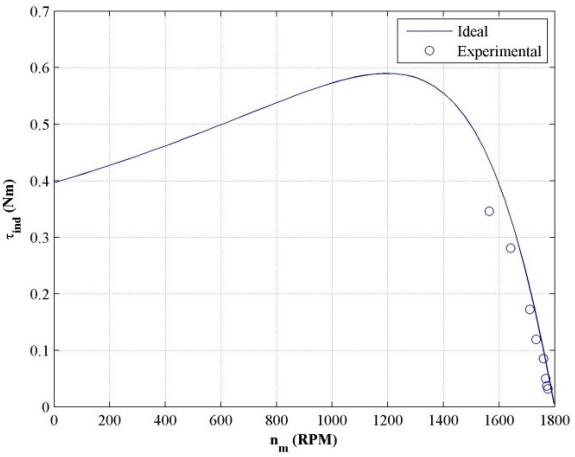

Figure 2. Induction-Motor Torque-Speed Characteristic

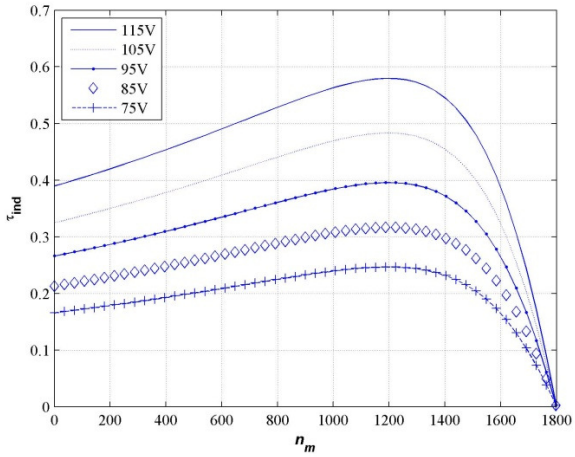

Figure 3. Torque-Speed Characteristic for Different Voltages

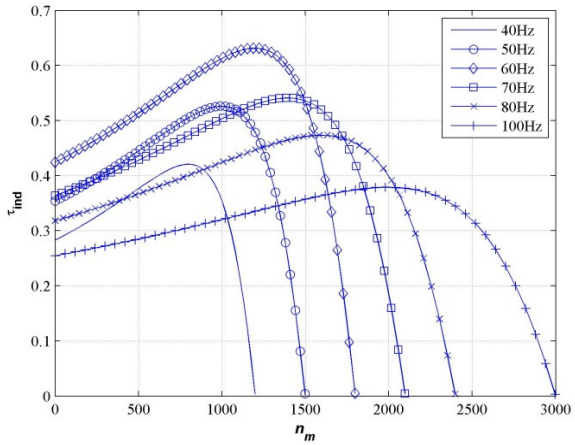

Figure 4. Torque-Speed Characteristic for Different Frequencies

System Setup and Experimental Data

In order to validate the simulation results, it is usually necessary to create an experimental setup capable of operating the motor at different load conditions, while monitoring the corresponding variables. A Hysteresis Brake was used for loading the motor. This device requires a regulated current source to produce a linearly proportional torque. Torque and speed sensors were used with their proper signal conditioning.

A variable-voltage AC power supply was an important piece of equipment in the setup. The Fluke-41B power analyzer provided an effective means to monitor voltage, current, power (real and reactive) and *p.f.* It provided valuable harmonic analysis data. Data acquisition and control were automated via traditional computer interface capabilities using LabVIEW software. Figure 5 shows a block diagram of the system and its physical setup.

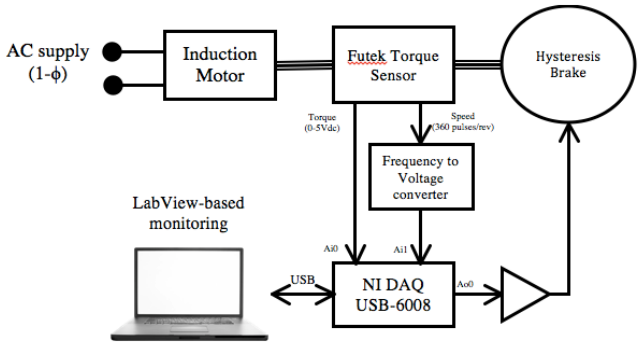

Figure 5(a). Block Diagram of the Experimental Setup

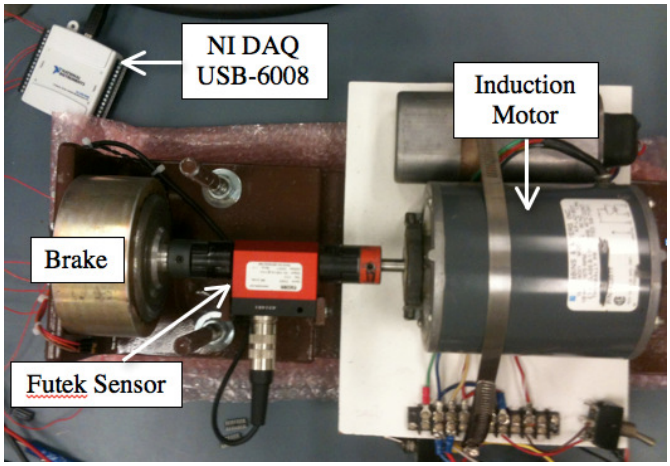

Figure 5(b). Motor-Brake Experimental Setup

Power Consumption

With the model of Figure 1 in mind, it is important to understand the power flow of a single-phase induction motor in order to analyze the data collected experimentally and validate simulation results. The calculated input power from Equations (2) and (3) corresponds to the power consumption of the motor, where V is the input voltage. Then, the first type of loss appears as stator copper loss, which corresponds to the power dissipated through the stator resistance, R_1. The power present in the air-gap is dissipated through the rotor resistance and is defined as P_{AG} in Equation(4). After some power is lost in the rotor, P_{RC}, the remaining power corresponds to the power converted from electrical to mechanical (P_{conv}); see Equations (5) and (6). The output and rotor powers are then given by Equations (7) and (8). Using the induction-motor parameters presented in Table 1, the motor was simulated under three different loading conditions in order to find the power consumption, the output power and the power converted from electrical to mechanical. These simulations were compared with the results obtained experimentally for model verification and are presented in Figure 6. These results demonstrate the validity of the mathematical model including the identified motor parameters.

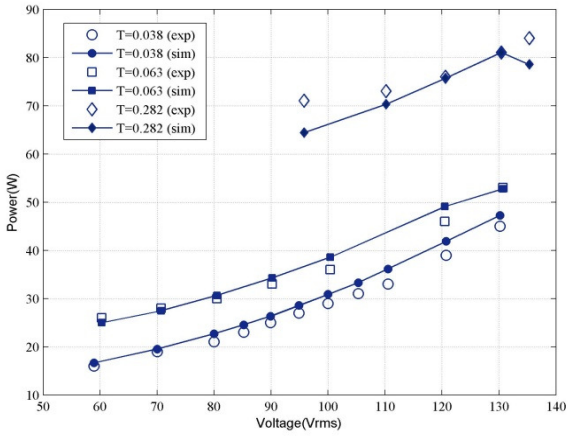

Figure 6. Power Consumption under Different Loading Conditions

Moreover, the model was validated through the experimental results obtained for the 120V, 100V and 80V voltage levels. Each voltage condition was tested over the torque range allowed by the motor. As the load increases, the speed and the slip change. Using these conditions, the values of R and L were determined for each case to conduct the simulations. The speed was measured experimentally and was then used to calculate the output power generated by the motor. In addition, the speed was used to calculate the slip used for the simulations. The results are presented in Figures 7-10.

$$P_{in} = VI\cos\theta \tag{2}$$

$$I = \frac{V}{R_1 + jX_1 + 0.5Z_F + 0.5Z_B} \tag{3}$$

$$P_{AG} = P_{AG,F} - P_{AG,B} \tag{4}$$

$$P_{conv} = P_{in} - P_{RCL} \tag{5}$$

$$P_{conv} = (1 - s)P_{AG} \tag{6}$$

$$P_{out} = \tau_{load}\omega_m \tag{7}$$

$$P_{rot} = P_{conv} - P_{out} \tag{8}$$

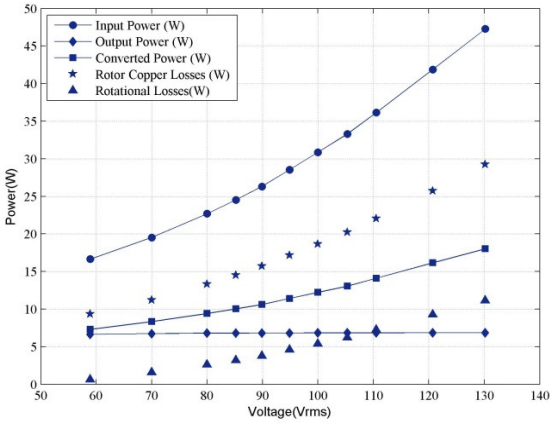

Figure 7. Power-Flow Representation over the Speed Range of Operation when Load is 0.038Nm

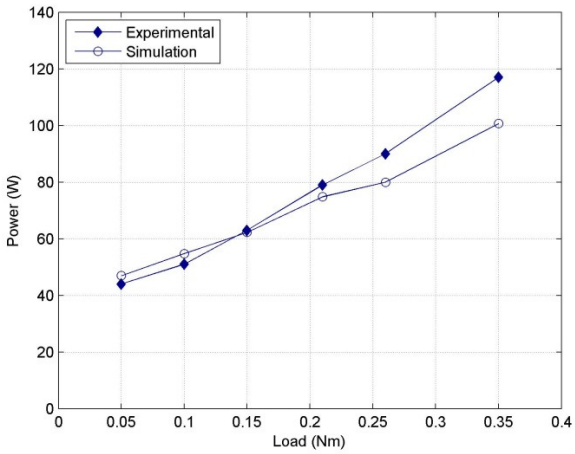

Figure 8. Power Consumption at 120Vrms

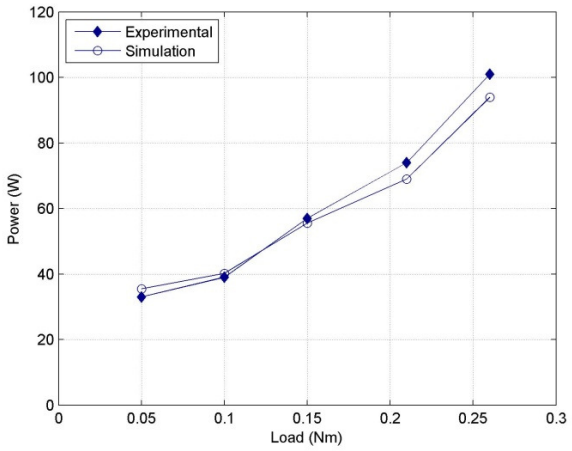

Figure 9. Power Consumption at 100Vrms

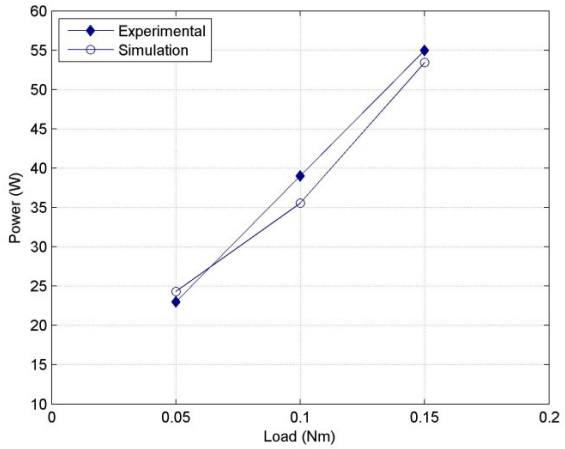

Figure 10. Power Consumption at 80Vrms

Energy Efficiency

The efficiency of the induction motor depends on several design parameters and factors that are part of the manufacturing process [7]. The motivation for producing high-efficiency motors is to reduce the operational costs of the machines over time. This study intended to develop a strategy for characterizing induction motors through simulations and experimental results, with the ultimate goal of finding the efficiency of the motor over a possible range of operation. In the previous section, the results showed the performance of the motor from a power-consumption point of view.

The efficiency results, experimental and simulated, obtained for a variation of the supply voltage and maintaining the operating frequency at 60Hz, are presented in Figure 11. Under these conditions, when the motor is operated near its rated condition (higher load and rated voltage), it achieves the most efficient mode of operation, as expected. Thus, notice that once again the steady-state model is a good approximation of the induction motor.

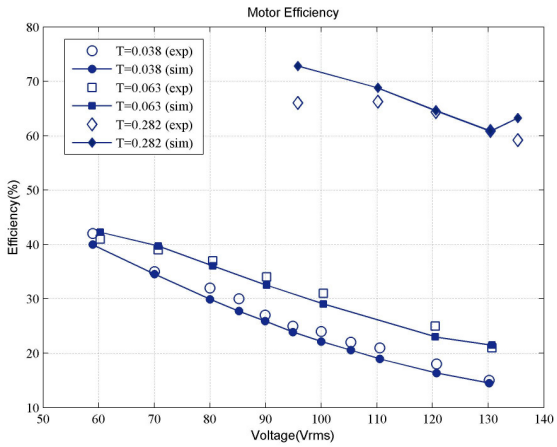

Figure 11. Efficiency under Different Loading Conditions (Operating at 60Hz)

Optimum Mode of Operation

The phase-control technique (control of the conduction angle) has a negative impact on the performance of the system due to the inherent presence of harmonics [8]. The Total Harmonic Distortion Ratio (THD-R) increases with the increment of the conduction angle. In addition, it was observed that when the motor was operating at certain voltages, and the load was increased, the THD-R also increased and the overall performance of the system diminished. Experimental tests were carried out to find the effects of this degradation on the efficiency of the motor under different loading conditions. The data presented in Table 2 show the experimental results using phase control over a range of loads, while operating at 100V.

Table 2. Experimental Results – Phase Control Operating at 100 V

Load (Nm)	n_m (rpm)	P_{out} (W)	P_{in} (W)	η (%)	THD-R (%)
0.05	1706	8.9326	36	24.81276	29.0
0.10	1674	17.5301	49	35.77569	29.2
0.15	1642	25.7925	62	41.60077	29.9
0.21	1606	35.3178	76	46.47077	30.7
0.26	1528	41.6031	104	40.00295	32.5

Notice the increase in THD-R as the load increases. Also, at the higher load (0.26Nm), there is a decrease in efficiency. This is because this loading condition is beyond the appropriate loading of the motor when operating at 100V. The results are shown in Figures 12 and 13 for the motor operating at 120V and 100V, respectively. In this configuration, the magnitude of the voltage is controlled by the input AC signal before it is passed through the rectifier. The frequency of the voltage applied to the motor after the full-bridge inverter depends on the modulating signal used for the PWM generator.

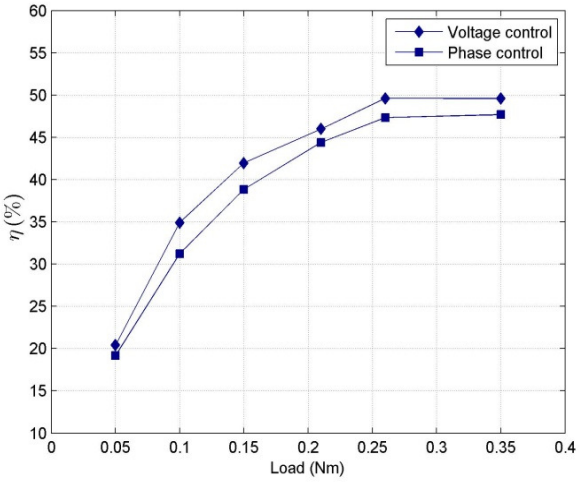

Figure 12. Efficiency at 120V

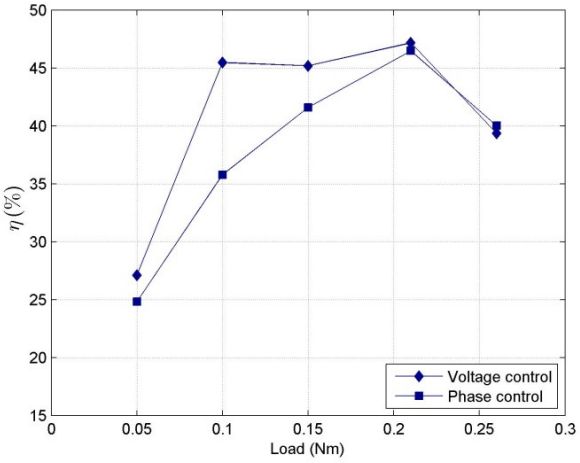

Figure 13. Efficiency at 100V

Finally, the three control schemes were compared by means of simulation (see Figure 14). It was found that the most efficient technique over the range of loading conditions, at rated values, was the variable-frequency scheme, where an inverter was employed. The PWM signal of the inverter can be modified depending on the application. If the frequency of the modulating signal is changed, the range of motor speed can be changed as well. This is a characteristic that is not possible via phase-control or voltage-control schemes. Matlab/Simulink was used to simulate the full-bridge inverter where the power devices were switched using PWM signals (see Figure 15). The inverter produces AC signals of a frequency dependent on the PWM signal. The amplitude of the AC signal was controlled by the magnitude of the DC signal at the input of the inverter [1]. The motor was modeled as an RL circuit, since the purpose of the study was to analyze the performance in the steady state. The resistor, R, corresponds to the losses in the stator and rotor losses, and the inductance corresponds to the main winding inductance [9], [10]. The resistor, R, would depend on the slip at which the motor is operated. The slip depends in the voltage and load applied to the motor. To analyze the motor using this model was necessary in order to define the operating conditions (speed and load) in order to find the slip through the torque-speed characteristic of the motor.

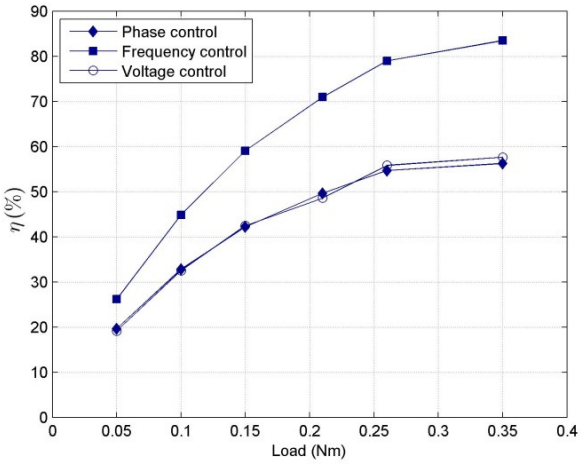

Figure 14. Efficiency under Different Loading Conditions

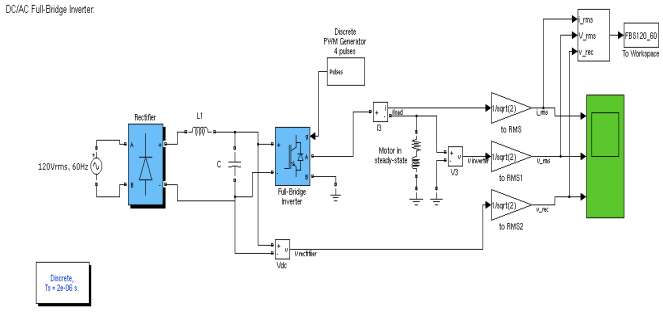

Figure 15. Full-Bridge Inverter Implementation in Simulink

The signals presented in Figure 16 show an example of the current and voltage output from the inverter to the motor in the steady state.

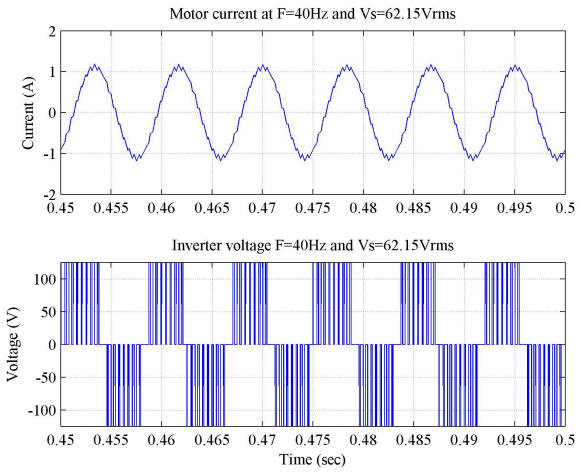

Figure 16. Example of AC Signals Generated by the Inverter

Fan Application

In variable airflow applications, it is common to use mechanical control devices like dampers while the motor continues to run at its rated power. This mode of operation is not efficient from an energy savings point of view since the power consumed is always constant, regardless of the desired airflow. As presented by Mohan et al. [1], the load torque in a fan application is proportional to the square of the speed, according to Equation (9), and the power consumed is proportional to the cube of the speed:

$$T_L = k_1 n_m^2 \tag{9}$$

where $k_1$is proportionality constant.

For this current study, a fan curve was assumed to be $k_1=8.546x10^{-8}$. Figure 17 illustrates the torque-speed characteristic of the motor at different operating voltages as well as the fan load curve. The intersection points of the fan curve with each of the corresponding motor curves signify the operating points for the fan at particular speeds. Each speed produces a specific air flow.

The theoretical results presented in Table 3 show the torque, speed, corresponding slip, power consumed and generated along with the efficiency of the motor at each of the intersecting points (fan operating points) (see Figure 17). In addition, the power savings compared to the use of dampers is calculated using Equation (10) and included in Table 3.

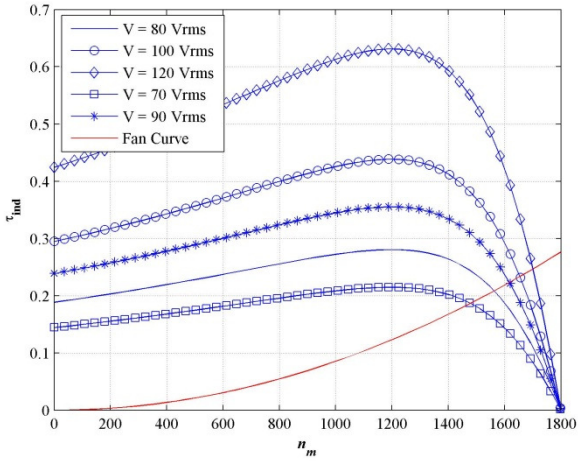

Figure 17. Variable-Voltage Motor Characteristic and a Fan Load

$$P_s = \frac{P_{rated} - P_{control}}{P_{rated}} x100 \tag{10}$$

Table 3. Operating Conditions of Fan at Different Speeds due to Voltage Control

V (V)	T (Nm)	n_m (rpm)	s (%)	P_{in} (W)	P_{out} (W)	η (%)	Pf	P_s (%)
70	0.186	1476	0.180	56.93	28.780	50.55	0.73	32.76
80	0.209	1576.4	0.132	65.04	34.147	52.50	0.75	23.19
90	0.224	1617.1	0.101	71.34	37.848	53.06	0.73	15.76
100	0.234	1654.2	0.081	76.41	40.534	53.04	0.70	9.77
120	0.247	1700.2	0.055	84.68	44.047	52.01	0.64	0

The data presented in these tables makes it abundantly clear that operating the motor at lower speeds, when less air flow is called for by the application, yields energy savings. Notice that the torque levels at each operating point is within the 100% load range of the motor. This is the reason why the efficiency and the power factor of the motor maintain an almost constant level, with minimum differences among the operating points.

Likewise, the variation of line frequency for speed control can be evaluated using the same methodology; this time, though, using the torque-speed characteristic curve of the motor at different operating frequencies versus the fan curves (see Figure 18). Table 4 contains the obtained theoretical results. It was found that the performance of the motor using the variable- frequency drive was superior to voltage control (see Figure 19). However, beyond the synchro-

nous speed, the motor consumes more power and, therefore, the power savings are negative (see Table 4).

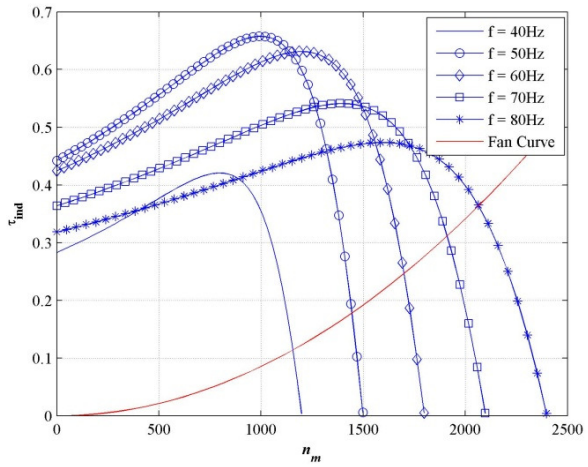

Figure 18. Variable-Frequency Motor Characteristic and a Fan Load

Table 4. Operating Conditions of Fan at Different Speeds due to Frequency Control

f (Hz)	V (V)	T (Nm)	n_m (rpm)	s (%)	P_{in} (W)	P_{out} (W)	η (%)	Pf	P_s (%)
40	80	0.114	1156	0.036	15.72	13.825	85	0.59	81
50	100	0.179	1445	0.036	37.7	27.012	64	0.70	55
60	120	0.247	1700	0.055	69.88	44.047	63	0.64	17
70	120	0.312	1911	0.090	101.3	62.443	62	0.70	-20
80	120	0.365	2065	0.139	116.1	78.813	68	0.76	-37

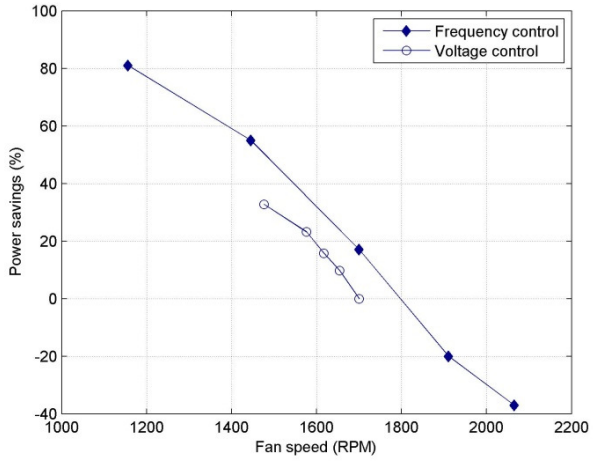

Figure 19. Power Savings Comparison: Voltage Control and Frequency Control

It is important to emphasize that the mathematical model presented here does not include the effects of harmonics. When the motor is operated using the variable-frequency drive, some harmonics are present in the voltage and current signals. The result of this is the mismatch in the power consumption of the motor at rated values (120V, 60Hz) for the two cases presented in Tables 3 and 4. However, it was also noticed that the calculated power factor using the mathematical model, and the one found through simulations, was the same. Therefore, the mismatch on power consumption was due to a lower current present in the motor.

Conclusion

The SPIM was successfully modeled for its steady-state operation in using the equivalent circuit method and experimentally determining the motor parameters. Test methodologies were developed and utilized to further validate the model and utilize it as an assessment tool for the efficiency of control schemes.

Three different speed-control schemes were considered when studying the performance of the motor under different loading conditions. It became evident that the high THD produced by the phase controller had a significant negative impact on motor performance, due to excessive power losses. Moreover, using the steady-state model, the full-bridge inverter was simulated as a variable-frequency drive and compared to the phase and voltage control schemes. It was found that the efficiency of the overall system was improved by approximately 25% at high loading conditions. However, at low loading conditions, the three techniques yielded a low efficiency of about 30%. It became clear that operating conditions may require changing the control scheme.

It is worth emphasizing that while PWM methodologies are usually embedded in numerous motor drives for their positive impact on the efficiency of the drives, the overall control scheme still needs to be evaluated carefully for its overall efficiency.

The fan application was studied for voltage control and variable-frequency control. These two schemes were chosen because of their higher efficiency compared to phase control. The variable-frequency drive yielded better results from an energy efficiency point of view. In addition, it is important to note that the variable-frequency drive works for a wider range of speeds, resulting in more versatility for the fan application. Thus, in some applications it might be necessary to have several options for the airflow and a wider range of speed would be needed. However, very high speeds may require changing the control scheme.

References

[1] Mohan, N., Undeland, T., & Robbins, W. (1998). *Power Electronics: Converters, Applications, and Design*. New York: John Willey & Sons, Inc.

[2] Schneider Electric. Unlocking Energy Efficiency - Management and Control is the Key. Retrieved from http://www.schneider-electric.co.il/documents/solutions/146-root-8-ee_white-paper.pd

[3] Latt, A. Z., & Win, N. N. (2009). Variable Speed Drive of Single Phase Induction Motor Using Frequency Control Method. *Proceedings of International Conference on Education Technology and Computer ICETC ,* (pp. 30-34, 17-20).

[4] Ahmed, N., Amei, K., & Sakui, M., (2000). AC chopper voltage controller-fed single-phase induction motor employing symmetrical PWM control technique. *Electric Power Systems Research*, *55*, 15-25.

[5] Yildirim, & Bilgic, M., (2008). PWM AC Chopper Control of Single-Phase Induction Motor for Variable -Speed Fan Application. Proceedings of *Industrial Electronics, IECON 34th Annual Conference of IEEE*, (pp. 1337-1342).

[6] Chapman, S. (2005). *Electric Machinery Fundamentals.* New York: McGraw-Hill.

[7] Amin, B. (2002). *Induction Motors: analysis and torque control*. New York: Springer.

[8] Sankaran, C. Effects of harmonics on Power Systems. EC&M Magazine. Retrieved from http://ecmweb.com/mag/electric_effects_harmonics_power_2

[9] Hamad, S. H., Bashi, S. M., Aris, I., & Mailah, N. F. (2004). Speed Drive of Single-Phase Induction Motor. *National Power & Energy Conference (PECon). Proceedings, Kuala Lumpur, Malaysia,* (pp. 121-125, 29-30).

[10] Li, H., & Curiac, R. (2010). Motor Efficiency, Efficiency Tolerances and the Factors That Influence Them. *Petroleum and Chemical Industry Conference (PCIC). Record of Conference Papers Industry Applications Society 57th Annual,* (pp. 1-6, 20-22).

Biographies

JUAN GALLEGO-CALDERON is currently a Ph.D. student at the DTU Wind Energy department, The Technical University of Denmark. He received his MS degree (Electrical Engineering, 2012) from California State University Fresno, CA. His present research interests are in electromechanical modeling, control systems, simulation of dynamical systems, multi-body dynamics and power systems in wind energy. He can be reached at jugc@dtu.dk

NAGY BENGIAMIN is a Professor of Electrical Engineering at California State University Fresno, CA, MEngr (Systems Engineering, 1976) from Carleton University, and Ph.D. (Electrical Engineering, 1979) from The University of Calgary, Canada. Dr. Bengiamin's current interests are in power systems, power electronics, and control systems. He is a senior member of IEEE. He can be reached at bengiami@csufresno.edu